

Spontaneously localized photonic modes due to disorder in the dielectric constant

Y. Kodriano,¹ D. Gershoni,^{1,*} E. Linder,¹ B. Shapiro,¹ M. E. Raikh,²
J. P. Reithmaier,³ S. Reitzenstein,⁴ A. Löffler,⁴ and A. Forchel⁴

¹*Department of Physics, Technion—Israel Institute of Technology, 32000 Haifa, Israel.*

²*Department of Physics, University of Utah, Salt Lake City, Utah 84112, USA.*

³*Technische Physik, Institute of Nanostructure Technologies and Analysis,
Universität Kassel, Heinrich-Plett-Str. 40, 34132 Kassel, Germany.*

⁴*Technische Physik, Universität Würzburg, Am Hubland, D-97074 Würzburg, Germany.*

We present the first experimental evidence for the existence of strongly localized photonic modes due to random two dimensional fluctuations in the dielectric constant. In one direction, the modes are trapped by ordered Bragg reflecting mirrors of a planar, one wavelength long, microcavity. In the cavity plane, they are localized by disorder, which is due to randomness in the position, composition and sizes of quantum dots located in the anti-node of the cavity. We extend the theory of disorder induced strong localization of electron states to optical modes and obtain quantitative agreement with the main experimental observations.

PACS numbers: 78.67.Hc., 42.55.Dd, 78.55.Cr, 68.37.Uv.

I. INTRODUCTION

Localization of a photonic mode by disorder in a statistically uniform and isotropic medium has been studied for more than two decades¹⁻⁴, both in the optical and microwave spectral ranges. In this paper we propose and demonstrate a new mechanism for disorder induced strong three dimensional (3D) localization of light. We achieved this in planar microcavities (PMCs), containing a layer of strain-induced self-assembled quantum dots (QDs)⁵⁻⁷. The dispersion of light in the PMC plane is modified by the distributed Bragg reflectors (DBRs) that trap the modes in perpendicular direction to the cavity plane. The QDs constitute an active material which, under proper excitation, emits photons, due to recombination of QD confined excitons^{8,9}. Randomness in the QDs in-plane position, composition and sizes produces fluctuations in the system's dielectric constant. This randomness provides the necessary “attractive potential”, which, together with the modified dispersion, brings about strong photon localization in the PMC plane. Our novel mechanism differs from previous studies, since it provides genuine disorder-induced localization rather than leaky (resonant) modes¹⁻⁴. It also differs from the “transverse localization”¹¹, where the wave freely propagates in one direction while being trapped, by disorder, in the transverse direction¹². We directly demonstrate the 3D localization of the photonic modes by measuring their photoluminescence (PL) intensity distribution.

It is worthwhile to emphasize from the start that the comparatively small size of the excitation spot (30 μm , or smaller) plays a crucial role in the interpretation of the experimental data. The point is that *in the absence of disorder* the shape of the PL spectrum emerging from the cavity is quite sensitive to the size of the excitation spot. If the size is sufficiently small, the PL spectrum becomes

very narrow, in marked difference with the broad shoulder predicted by the standard ‘basic cavity physics’. If there had been no disorder, the experimental conditions of our paper would have resulted in an extremely narrow PL peak. The significant broadening of the spectrum, as observed in our experiment, is due entirely to disorder. The broadening occurs both towards frequencies below and above the cavity frequency (localized and resonant photonic modes, respectively). All this will be discussed in detail in the theoretical part of the paper.

II. EXPERIMENTAL

Our sample was grown by molecular beam epitaxy on a [1,0,0] oriented GaAs substrate. The sample consists of a PMC formed by a GaAs one-wavelength resonator, sandwiched between DBRs made from 23(26) top (bottom) alternating GaAs and AlAs quarter-wavelength-layer pairs. As an active material in the resonator's anti-node, a single strain-induced self-assembled $\text{In}_{0.3}\text{Ga}_{0.7}\text{As}$ QDs layer with average density of 5×10^9 QDs per cm^2 is used¹³. The use of such composition results in large and asymmetric QDs with typical lengths and widths of about 100 and 30 nm respectively, as can be seen in the inset to Fig. 1a.

We used two methods to study the PMC. a) a diffraction limited confocal optical scanning microscopy (a $\times 60$ objective with numerical aperture of 0.85, obtaining spatial resolution of $\sim 0.7 \mu\text{m}$). b) a near field scanning optical microscopy (NSOM- Nanonics Cryoview 2000TM with spatial resolution of $\sim 0.25 \mu\text{m}$). By applying either method we measure the lateral distribution of the electromagnetic field above the sample surface. Two modes of excitation were used. In the first, the excitation was focused to a diffraction limit by the collecting objective¹⁴. In the second (the only one used for NSOM), the

excitation was focused at an oblique angle to a spot diameter of about $30 \mu\text{m}$. Due to the high energy used for the excitation (632.8 nm light of a HeNe laser) the images produced by the two excitation modes were almost identical. In Fig. 1a we present PL spectrum (upper, black solid line) from a single point on the surface of the PMC sample together with a PL spectrum which was taken from the same sample (lower, solid blue line) after the upper DBR mirror was completely etched. The spectrally broad blue PL line is centered at 1.33 eV and has full width at half maximum (FWHM) of approximately 10 meV. This spectral line results from s-shell electron-hole recombination within the inhomogeneous population of QDs of various sizes and compositions. The radiative linewidth of a QD is $\sim 2\mu\text{eV}$ ⁹.

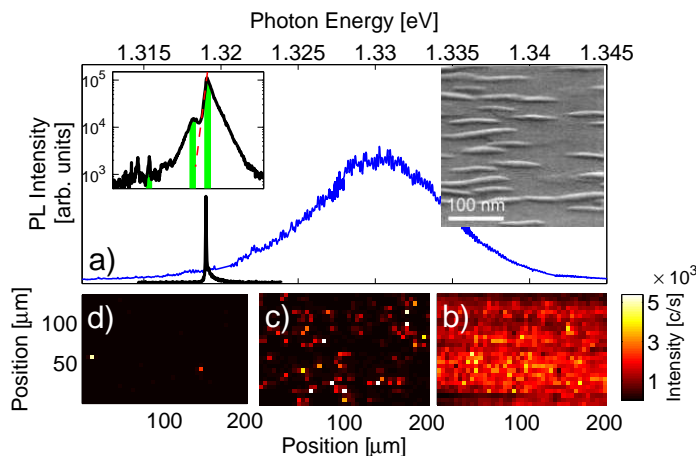


FIG. 1: a) PL spectrum of the PMC with (solid black line) and without (solid blue line) the upper DBR. The left inset represents spatially integrated PL spectrum from a $135\mu\text{m} \times 200\mu\text{m}$ area on the sample surface. b)-d) selective wavelength images of the area for 3 different spectral domains indicated by the green zones in a). The right inset is a scanning electron micrograph of the QDs layer.

The rather symmetrical shape of the spectral line indicates that charge carriers are not distributed thermally between the QDs. Therefore, it is quite safe to assume that the spectrum accurately represents the actual energy distribution of the emission from individual QDs. The spectrally sharp PL line in the figure is centered at 1.319 eV and has FWHM of $80 \mu\text{eV}$. As we explain below, in a disorder free PMC this line width should have been about an order of magnitude narrower due to the finite excitation area and diffraction limited collection spot.

The asymmetric spectral shape of the line and its actual linewidth which represents a Q-factor of ~ 15000 , in similarity to earlier measurements⁵⁻⁷, are due to the disorder in the dielectric constant as we quantitatively show below.

In the left inset to Fig. 1a we present on a semi logarithmic scale a spatially integrated ('far field') PL spectrum from a $135\mu\text{m}$ wide $\times 200\mu\text{m}$ long area on the sample's surface. The spectrum was obtained by summing up large number of individual PL spectra, each obtained

from a diffraction limited areal spot. The dominating spectral feature is a large, asymmetrically broadened line around the energy of the PMC mode. The line decays exponentially towards lower energies with a characteristic energy of $150 \pm 30\mu\text{eV}$. Towards higher energies the line decays with a characteristic energy of $380 \pm 30\mu\text{eV}$. The ratio between these characteristic energies agrees well with the prediction of our theoretical model for the disorder in the dielectric constant (see below).

In Figs. 1b-1d selective wavelength images of the scanned area are presented. The spectral domains which are used for each image are indicated by the green zones imposed on the 'far field' spectrum in Fig. 1a. The image in Fig. 1b is obtained within a 0.5 meV energy window containing the PMC mode. It shows almost evenly distributed emission from the surface. In contrast, the image in Fig. 1c, which is obtained within a 0.5 meV window, 1 meV below the PMC mode, shows emission emerging from randomly distributed spots on the surface. Likewise, the image in Fig. 1d, which is obtained from energy window of same width, located 3 meV lower, shows only 2 bright centers, from which all the emission results.

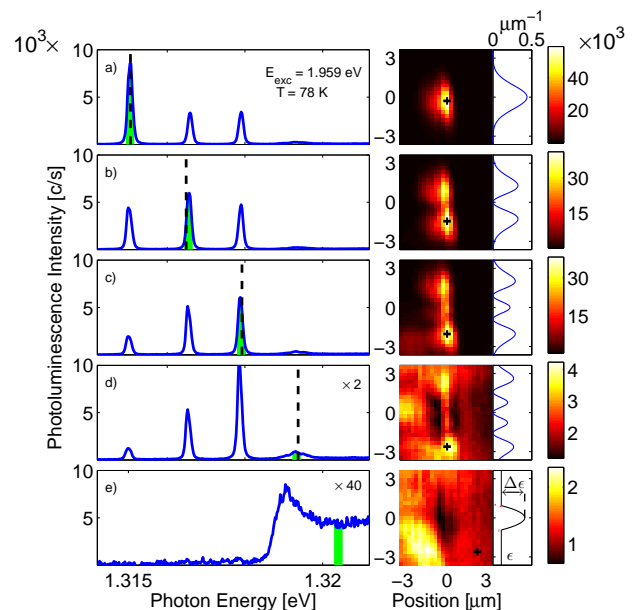


FIG. 2: a)-e) middle panels - selective wavelength NSOM images of an area in the vicinity of the lowest energy mode observed in Fig. 1. The spectra (left panels) are obtained from the brightest area pixels indicated by the + signs on the images. The green areas on the spectra, indicate the spectral domains used for generating the images. The right panels represent analytically calculated 1D intensity distributions of the confined optical modes obtained by solving Eq. (2) with the parabolic dielectric constant fluctuation model presented in the right panel of e) where $\Delta\epsilon/\epsilon = 0.7\%$ and ϵ the dielectric constant of GaAs. The calculated mode energies are presented by dashed vertical lines on the spectra to the left.

In Fig. 2 we turn our attention to one of the low energy electromagnetic modes seen in Fig. 1d. Such localizing

centers were observed in various mode energies and various locations on the sample surface. In the right panels of Figs. 2a-2e, we display selective wavelength images obtained by scanning the Aluminum coated fiber tip of our NSOM microscope in tapping mode over the sample surface. The corresponding spectra in the left panels, are obtained from the brightest area pixels indicated by the + signs on the images. The green areas on the spectra indicate the spectral domains used for generating these images. These spectra and corresponding images reveal the following observations: Four different localized photonic modes are observed at energies below that of the PMC mode. Each mode is composed of two cross linearly polarized equally intense components (not shown). The components are $\sim 80\mu\text{eV}$ apart and the lower energy one is polarized along the $[0,-1,1]$ direction¹⁰. The lowest energy mode is about 5 meV below the energy of the PMC mode. The in-plane spatial intensity distribution of this mode, as depicted by the image in Fig. 2a, is node-less, and has an elongated shape oriented along the $[0,-1,1]$ crystallographic direction, along which the QDs are also elongated (see inset to Fig. 1). The mode dimensions are roughly $3 \times 2\mu\text{m}^2$. The peak intensity is about 40 times stronger than that of the PMC mode. The next three images in Fig. 2b, c and d, present elongated spatial intensity distributions composed of one, two and three nodes, respectively. Each mode's energy is ~ 1.5 -2 meV higher than the energy of the preceding mode. The selective wavelength image in Fig. 2e is obtained at an energy window, which resides on the higher energy side of the PMC mode. It displays evenly distributed emission from everywhere except from the actual locus of the localized modes, where extended modes are forbidden. The magnitude and shape of the spot from which emission at this wavelength is missing is an estimate for the spatial extent of the region which localizes the optical modes. The region is comparable in shape and size to the most localized, lowest energy mode. The localized modes are insensitive to temperature and excitation density variations, hence they do not result from thermal or non-linear effects. The emission is linear with the excitation density between 1 - 10^6 Watt/cm². Increasing the temperature from 10 to 80K results in a small, rigid, red spectral shift, as expected from the temperature dependence of the material bandgap.

III. THEORY

Since the sizes of the spots in Fig. 2b-2d significantly exceed the size of an individual QD, the only way to account for the experimental observations is to assume that each spot corresponds to a *localized* electromagnetic mode. Therefore the low frequency tail of the PL spectrum in Fig. 1a should be interpreted as a tail of localized modes with energies below that of the PMC mode, ω_c , similar to the tail of localized electron states formed below the band-edge due to disorder^{15,16}. To demonstrate

how the presence of a cavity leads to the in-plane trapping, we consider the scalar wave equation corresponding to the frequency Ω :

$$\frac{d^2\Psi}{dz^2} + \nabla_{\rho}^2\Psi + \frac{\Omega^2}{c^2} \left[\varepsilon_0 + \delta\varepsilon(\boldsymbol{\rho}, z) \right] \Psi = 0, \quad (1)$$

where ε_0 is a uniform dielectric constant inside the cavity, $\boldsymbol{\rho} \equiv (x, y)$, and $\delta\varepsilon(\boldsymbol{\rho}, z)$ is the perturbation due to the randomly positioned QDs that reside in a narrow layer, of width $\delta z \sim 5$ nm, in the middle of the cavity. Let us emphasize that an individual QD is much too small to be able to trap a photon. Actually, in the continuum description employed in Eq. (1) individual QDs are not resolved. What matters are the fluctuations in the areal density of the QDs, which manifest themselves in fluctuations of the dielectric constant $\delta\varepsilon$. Since the electromagnetic modes are confined in the z -direction to a much shorter length than in the plane, the function $\Psi(\boldsymbol{\rho}, z)$ can be factorized as $\Phi(\boldsymbol{\rho})\cos(\pi z/d)$, where d is the cavity width, and $\Phi(\boldsymbol{\rho})$ satisfies the equation

$$-c^2\nabla_{\rho}^2\Phi - \Omega^2\delta\varepsilon(\boldsymbol{\rho})\Phi = -\varepsilon_0(\omega_c^2 - \Omega^2)\Phi. \quad (2)$$

In this equation, $\delta\varepsilon(\boldsymbol{\rho})$ is the effective in-plane fluctuation of the dielectric constant obtained from $\delta\varepsilon(\boldsymbol{\rho}, z)$ by averaging over the z -distribution of the cavity mode intensity, namely, $\delta\varepsilon(\boldsymbol{\rho}) = \frac{2}{d} \int_{-d/2}^{d/2} \delta\varepsilon(\boldsymbol{\rho}, z) \cos^2(\pi z/d)$. The analogy between Eq. (2) and the Schrödinger equation makes it clear that, for positive $\delta\varepsilon(\boldsymbol{\rho})$, Eq. (2) admits localized solutions, with frequency Ω smaller than the cavity frequency $\omega_c = 2\pi c/d\sqrt{\varepsilon_0}$. Thus, even a small enhancement in $\delta\varepsilon(\boldsymbol{\rho})$ acts as an attractive potential localizing the mode laterally. To substantiate that this mechanism of trapping is relevant to our experimental observations, we note that the spatial intensity distributions and the energies of the modes in Fig. 2 are quite accurately fitted by solving Eq. (2) using a one dimensional parabolic model ($\delta\varepsilon(x) = \Delta\varepsilon[1 - (\alpha x)^2]$, $|\alpha x| \leq 1$) describing a local fluctuation in the dielectric constant (see Fig. 2e, right panel, where the best fitted values are $\alpha = 0.3\mu\text{m}^{-1}$ and $\Delta\varepsilon/\varepsilon_0 = 0.7\%$). This agreement, and the fact that even in the case of the most localized modes, differently polarized components have almost the same energy, justifies the use of the scalar approximation.

To find the shape of the tail of the localized modes distribution, we have to specify the disorder ‘‘potential’’, $\delta\varepsilon(\boldsymbol{\rho})$. The simplest possible model is the ‘‘white-noise potential’’ which amounts to treating the QDs as point-like resonant units, randomly distributed in the plane (this simple model does not describe the anisotropy observed in the inset of Fig. 1 as discussed below). Fluctuations in the local dielectric constant are given as

$$\delta\varepsilon(\boldsymbol{\rho}) = A \int \frac{\delta N_{\omega}(\boldsymbol{\rho})}{\omega^2 - \Omega^2}, \quad (3)$$

where $\delta N_{\omega}(\boldsymbol{\rho})$ is the deviation of the number of QDs (per unit area near $\boldsymbol{\rho}$), with resonance frequency in the

interval $d\omega$, from the average value $\bar{N}P_D(\omega)d\omega$. Here \bar{N} is the total areal density of the QDs, regardless of their frequency and $P_D(\omega)$ is the probability distribution of the resonance frequencies (the solid, blue line in Fig. 1).

To estimate the constant A , we consider the $\Omega \rightarrow 0$ limit and imagine that the entire layer consists of QDs, i.e. of $\text{In}_{0.3}\text{Ga}_{0.7}\text{As}$. In this case, the enhancement of the dielectric constant in the layer, as compared to the surrounding material of GaAs, is $(\varepsilon_{\text{InAs}} - \varepsilon_{\text{GaAs}}) \cdot 0.3$. This value should be multiplied by $\delta = 5/300$, which is the ratio of the QDs layer width (5 nm) to the cavity width (~ 300 nm). There is an extra factor of 2, since the QDs are located at the anti-node of the PMC mode. Thus, the effective enhancement, due to the presence of InAs, is $\Delta\varepsilon \cong 2.25 \times 10^{-2}$. The constant A can now be estimated from Eq. (3) as $A \cong 2.25 \times 10^{-2} S \omega_0^2$, where S is the typical area of a QD and $\omega_0 \approx \omega_c$ is the central frequency of the distribution $P_D(\omega)$. Note that the employed averaging in the z -direction, as well as our use of the scalar approximation is justified by the smallness of the parameter δ . Indeed, the effect of disorder-induced coupling between different cavity modes is proportional to δ^2 , whereas the effect of the QD layer on a given mode is proportional to δ .

The function $\delta N_\omega(\boldsymbol{\rho})$ is a complicated, random function of position $\boldsymbol{\rho}$ and frequency ω . Using the white-noise model for $\delta N_\omega(\boldsymbol{\rho})$ and Eq. (3), we obtain the probability $P\{\delta\varepsilon(\boldsymbol{\rho})\}$ for a particular realization $\delta\varepsilon(\boldsymbol{\rho})$ of the fluctuating part of the dielectric constant

$$P\{\delta\varepsilon(\boldsymbol{\rho})\} \sim \exp \left\{ -\frac{2\omega_c^2}{\bar{N}A^2} \left(\int \frac{P_D(\omega)d\omega}{(\omega - \Omega)^2} \right)^{-1} \int d^2\boldsymbol{\rho} [\delta\varepsilon(\boldsymbol{\rho})]^2 \right\} \quad (4)$$

Formally, the integral over ω in Eq. (4) diverges at $\omega \approx \Omega$. In this regard, it should be noted that the integral over ω is actually an approximation for a sum over discrete values, ω_i , of the resonant frequency of the dots in the relevant area (of order $1 \mu\text{m}^2$). The meaning of this area can be traced back to Eq. (3) which defines a macroscopic (albeit still fluctuating in space) dielectric constant. The spatial scale, over which $\delta\varepsilon(\boldsymbol{\rho})$ is changing, should be at least few times larger than the ‘‘microscopic’’ distances (size of the dots and their separation, of the order of $0.1 \mu\text{m}$). Thus, the minimal scale at which $\delta\varepsilon(\boldsymbol{\rho})$ can be meaningfully defined should be in the sub-micron range. We are interested in Ω below ω_c , i.e. in frequency which belongs to the tail of the distribution $P_D(\omega)$. A simple estimate shows that for such Ω the probability to encounter a dot with ω_i close to Ω is extremely small. Moreover, for such Ω the integral over ω in Eq. (4) can be, roughly, replaced by $(\omega_0 - \Omega)^{-2}$ (note that such a replacement would not be possible for Ω in the ‘‘bulk’’ of the probability distribution $P_D(\omega)$). The two equations, (2) and (4), define the statistical problem of finding the probability that a localized mode, in a given frequency interval, will be created. This problem is completely identical to the two-dimensional version¹⁷ of the problem of the tails of electron states in a ran-

dom potential^{15,16}. The final result for the probability $\mathcal{P}(\Omega)d\Omega dS$ to find a trap, in an area dS , which can support a localized mode in the frequency range $d\Omega$ can be presented as

$$\mathcal{P}(\Omega) \cong \frac{\varepsilon_0\omega_c}{\pi c^2} \exp \left[-32\pi \frac{\varepsilon_0 c^2}{A^2 \bar{N}} \frac{\omega_c - \Omega}{\omega_c} \cdot (\omega_0 - \Omega)^2 \right], \quad (5)$$

where the pre-exponential factor corresponds to the density of the PMC modes at frequencies $\Omega \gtrsim \omega_c$. Eq. (5) can be viewed as a qualitative interpolation between the maximal value of the modes density at $\Omega = \omega_c$, and the low-density ‘‘tail’’. A more detailed crossover behavior between the tail at $\Omega < \omega_c$ and $\mathcal{P} = \varepsilon_0\omega_c/\pi c^2 = \mathcal{P}_0$ at $\Omega \gtrsim \omega_c$ can be found in Ref. 18. Important is that this crossover is determined by a *single* scale of frequencies

$$\omega_t = \omega_c \frac{A^2 \bar{N}}{32\pi\varepsilon_0 c^2 (\omega_0 - \omega_c)^2}, \quad (6)$$

which follows from Eq. (5), so that in the tail region $\mathcal{P}(\Omega)$ can be rewritten as $\mathcal{P}(\Omega) \approx \mathcal{P}_0 \exp[-(\omega_c - \Omega)/\omega_t]$. In Eq. (6) we replaced $(\omega_0 - \Omega)$ by $(\omega_0 - \omega_c)$, since, experimentally, the difference $(\omega_0 - \omega_c)$ is much bigger than the tail width, ω_t .

With the above estimate for the constant A , Eq. (5) yields a characteristic energy of $100 \pm 70 \mu\text{eV}$ for the initial decay of the PL intensity below $\hbar\omega_c$. It agrees well with the measured value (dashed red line in the left inset to Fig. 1a). The relatively large uncertainty results from the uncertainties in the QDs density and their average area.

Up to now we have focused on explaining the PL spectrum tail for $\omega < \omega_c$. In this domain, the PL intensity, $I(\Omega)$, outside the cavity is simply proportional to the density of trapped modes, $\mathcal{P}(\Omega)$. In other words, the Ω -dependence of the light intensities inside and outside the cavity is the same for $\omega < \omega_c$. This is *not the case* for the domain of frequencies $\omega > \omega_c$ to which we now turn. To calculate $I(\Omega)$ in this domain, we start by recapitulating the basic microcavity physics, in the absence of disorder. In this case the emission spectrum is controlled by the Airy factor¹⁹

$$Ai(\Omega, \theta) = \frac{T}{|1 - r_1 r_2 \exp[2i\phi(\Omega, \theta)]|^2}, \quad (7)$$

where θ is the angle at which the radiation exits the cavity, $\Omega > \omega_c$ is the radiation frequency, r_1 (r_2) is the reflection amplitude from the upper (lower) Bragg mirror and $T = 1 - r_1^2$ is the transmission coefficient (r_1 and r_2 are taken to be real). The phase $\phi(\Omega, \theta) = \sqrt{\varepsilon_0}\Omega d \cos\theta/c$ is acquired in course of propagation between the boundaries $z = \pm d/2$. At frequencies, Ω , close to ω_c Eq. (7) has a sharp maximum at $\theta = \theta_\Omega$, where the angle θ_Ω is defined as

$$\theta_\Omega = \left[\frac{2(\Omega - \omega_c)}{\omega_c} \right]^{1/2}, \quad (8)$$

so that $Ai(\Omega, \theta)$ can be simplified to

$$Ai(\Omega, \theta) = \frac{T}{T^2 + 4\pi^2(\theta^2 - \theta_\Omega^2)^2}. \quad (9)$$

Note that condition $\theta = \theta_\Omega$ coincides with the dispersion law of the waveguided mode. This follows from Eq. (2) in the absence of disorder. Indeed, for in-plane wave vector, $q = \sqrt{\varepsilon_0}\Omega \sin \theta/c$, Eq. (2) yields $q \approx \sqrt{2\varepsilon_0\omega_c(\Omega - \omega_c)}/c$, leading to $\theta = \theta_\Omega$ for $\theta_\Omega \ll 1$.

It follows from Eq. (9) that the emission spectrum, $I(\Omega)$, has a form of a plateau, which corresponds to the basic microcavity physics. Indeed, integration over θ yields

$$I(\Omega) \propto \int_0^\infty d\theta \theta Ai(\Omega, \theta) = \frac{1}{8} \left[1 + \frac{2}{\pi} \arctan\left(\frac{2\pi\theta_\Omega^2}{T}\right) \right]. \quad (10)$$

The second term describes a slight smearing of the plateau near $\Omega = \omega_c$.

Let us consider now photons which exit at an angle θ , from some small collection spot. It is important to realize that there is a correlation between the angle θ and the average distance $L(\theta)$ (measured from the collection spot) at which the corresponding photons have been created. Indeed, a typical photon will bounce $1/T$ times before escaping the cavity. Therefore photons that bounce at angle θ and escape at the collection spot must be created at a distance

$$L(\theta) \sim T^{-1} d \tan \theta \approx \frac{\theta d}{T}. \quad (11)$$

Thus, the finite size of an *excitation* area can serve as an efficient cutoff for a maximal escape angle θ_m . Assuming a circular excitation area, of radius R , and choosing a small collection spot at the center of the circle, one finds a maximal escape angle

$$\theta_m = \frac{RT}{d}. \quad (12)$$

Of course, this relation is valid only if θ_m (and therefore R) is not too large, namely, it should be smaller than the maximal escape angle for a fully excited cavity. Since the angular cutoff translates into a frequency cutoff $\Omega_m = \omega_c(1 + \frac{1}{2}\theta_m^2)$ (see Eq. (8)), we arrive at the important conclusion that the frequency range of the collected photons can become very narrow, if the excitation area is small enough. In our experiment $T = 0.44 \times 10^{-4}$, $R \cong 30\mu$, so that the collected radiation constitutes a narrow peak at near ω_c , of relative width

$$\frac{\Omega_m - \omega_c}{\omega_c} = \frac{\theta_m^2}{2} = \frac{1}{2} \left(\frac{RT}{d} \right)^2 \approx 1 \times 10^{-5}. \quad (13)$$

Obviously, this peak can be replaced by a δ -function

$$I(\Omega) = I_0 \delta(\Omega - \omega_c). \quad (14)$$

Qualitatively, the meaning of Eq. (14) is that, due to the finite excitation spot, only the photons emitted normally to the mirror emerge outside the cavity. Quantitatively we note that the relative width of the experimentally measured PMC mode ($\approx 1 \times 10^{-4}$) is about an order of magnitude wider than the one calculated by Eq. (13). As we show below, this broadening and the actual spectral shape of the PMC mode, results from the disorder. The replacement of the step-like spectrum of the *clean* cavity (for infinite excitation spot) by the δ -function Eq. (14) (for finite excitation spot) does not affect the emission spectrum of *disordered* cavity in the domain $\Omega < \omega_c$. In this domain the dependence, $I(\Omega)$, is still determined by Eq. (5). However, in the domain $\Omega > \omega_c$, the δ -peak for the clean cavity gets broadened due to scattering of *extended modes* by the disorder.

In the presence of disorder, the above reasoning, which is based on the ray picture, is not applicable since *all* the solutions, $\Phi_\mu(\boldsymbol{\rho})$, of Eq. (2) corresponding to the eigenstates, Ω_μ , have components with $\mathbf{q} = 0$ (in the ray picture they correspond to rays with normal incidence to the microcavity plane). The amplitude of this component is given by $\int d^2\boldsymbol{\rho} \Phi_\mu(\boldsymbol{\rho})$. Therefore, the shape of the spectrum acquires the form $I(\Omega) = I_0 \mathcal{A}(\Omega)$ where the function $\mathcal{A}(\Omega)$ is defined as

$$\mathcal{A}(\Omega) = \sum_\mu \int d^2\boldsymbol{\rho} |\Phi_\mu(\boldsymbol{\rho})|^2 \delta(\Omega - \Omega_\mu). \quad (15)$$

We note that the function $\mathcal{A}(\Omega)$ as defined by Eq. (15) is normalized

$$\int_{-\infty}^{\infty} d\Omega \mathcal{A}(\Omega) = 1, \quad (16)$$

Thus, the disorder broadens the δ -peak (Eq. (14)) without changing its area. Note also, that the calculation of the spectral shape, $\mathcal{A}(\Omega)$, is formally reduced to the calculation of the spectrum of two-dimensional *exciton* absorption in the presence of a white-noise random potential. This calculation was done earlier in Ref. 20, where the zero-momentum components of the *exciton* states were selected by the matrix element for light absorption²⁰.

It is also important to note that the spectral shape, $\mathcal{A}(\Omega)$, is a function of the ratio $(\Omega - \omega_c)/\omega_t$, where ω_t is the same characteristic frequency, (Eq. (6)), which determines the spectral shape of the tail of the localized photon states. Indeed, deep in the tail, $(\omega_c - \Omega) \gg \omega_t$, all the trapped solutions, $\Phi_\mu(\boldsymbol{\rho})$, at a given $\Omega_\mu = \Omega$ are identical to each other, and Eq. (15) is essentially reduced to the density equation of the trapped modes $\propto \exp[-(\omega_c - \Omega)/\omega_t]$ (Eq. (5)).

In the opposite limit $(\Omega - \omega_c) \gg \omega_t$ the density of photon states is constant. Here, therefore, the decay of $\mathcal{A}(\Omega)$ is determined by the fall-off of the integral $\int d^2\boldsymbol{\rho} \Phi_\mu(\boldsymbol{\rho})$. This integral can be estimated to first order by perturbation expansion in $\delta\varepsilon(\boldsymbol{\rho})$. Thus it is proportional to $(\Omega - \omega_c)^{-1}$. Accurate calculation²⁰ yields

$\mathcal{A}(\Omega) \approx \omega_t/(\Omega - \omega_c)^2$. This way, the width of the emission spectrum was found to be $3.7\omega_t$.

The overall spectral shape of $\mathcal{A}(\Omega)$ was found in Ref. 20 by combining the normalized (Eq. (16)) low-frequency and high-frequency asymptotes. The calculated full width at half-maximum (FWHM) of the emission spectrum is $3.7\omega_t$, in excellent agreement with the experiment, where it is measured to be $3.5\omega_t$. The calculated ratio between the high energy and low energy slopes is 2:1 in very good agreement with the measured ratio of 2.5.

IV. DISCUSSION

While the white noise model is successful in explaining the initial drop of the density of localized modes, it cannot account for the experimental data in the deeper tail, starting around $\Omega = 1.318$ eV and below. It does not explain the non-monotonic decay of the probability as seen in Fig. 1a. It fails in predicting the observed multiplicity of confined modes which belong to the same localization region (Fig. 2), and it does not explain the anisotropy in the electromagnetic mode shapes.

The failure of the white noise model, for $\Omega < \omega_c$, is not surprising. Indeed, when the mode frequency becomes smaller, localization of the mode becomes tighter. Thus, various local features of the random potential - such as correlations in $\delta\varepsilon(\rho)$, the ‘‘granular’’ structure of the disorder and the inherent anisotropy of the system - become more important. Obviously, all these features are not captured by the entirely featureless, universal white noise model.

Proper account of these specific features of randomness might explain some of the data for the deeper Ω -tail. First, once correlations are introduced, the most probable deep fluctuation is no longer a fluctuation which captures one mode only. Second, the probability of finding a localized mode common to two localizing centers, rather than to one, may prevail at a given energy below the energy of the PMC mode. Indeed, localized modes between 1.317 eV and 1.318 eV always exhibit a spatial structure consisting of two bright spots separated by a dark region. This observation suggests existence of traps of a double-well shape. The origin of such traps, as well as the multimode traps in the deep tail (below 1.316 eV), may be traced to the granular nature of the disorder.

Although, on the average, the QDs are uniformly distributed, there exist configurations with several dots coming close to each other, within a distance of a dot size. Such rare configurations constitute more efficient traps than the white-noise fluctuations and therefore dominate in the deeper tail. The clusters of QDs are akin to clusters of potential wells in the Lifshitz model of a disordered electronic system^{21,22}. Thus, anisotropic QD clustering, can account for the shape and multiplicity of the strongly localized modes in the deeper tail. We are unable to make quantitative predictions for the density and spatial structure of these modes, since no comprehensive theory exists. Yet, we show that dielectric constant enhancement of order 1% over distance of order $1\mu m$, does account for the experimental observations (Fig. 2e).

In conclusion, we demonstrate disorder-induced trapped photonic modes in a microcavity with an embedded layer of QDs. In the lateral in-plane direction the modes are localized by spatial fluctuations of the dielectric constant due to randomness in the location and composition of the QDs. Our theory emphasizes the universal features of the trapping mechanism: the necessary combination of mirrors in the vertical direction and the lateral disorder. The theory quantitatively estimates the characteristic energy by which the PL intensity decays below the PMC mode. Since the non universal, system-specific details of the randomness are not accurately known, the spatial shapes and energies of the modes deeper in the energy tail, are qualitatively discussed only.

In addition we show both experimentally and theoretically that if the size of the excitation spot is sufficiently small, as it is in confocal and near field scanning microscopy, the microcavity emission spectrum becomes very narrow, in marked difference with the prediction of the standard cavity considerations, which apply to uniform excitation. The disorder broadens this spectrum, as well. Thus, we quantitatively measure and calculate the disorder induced broadening below and above the cavity mode frequency.

Acknowledgments

This research is supported by the German Israel and by the Israeli Science Foundations (GIF and ISF) and by RBNI at the Technion.

* Electronic address: dg@physics.technion.ac.il

¹ D. S. Wiersma, P. Bartolini, A. Lagendijk, and R. Righini, *Nature* (London) **390**, 671 (1997).

² F. Scheffold, R. Lenke, R. Tweer, and G. Maret, *Nature* (London) **398**, 206 (1999).

³ A. A. Chabanov, M. Stoytchev, and A. Z. Genack, *Nature* (London) **404**, 850 (2000).

⁴ D. Laurent, O. Legrand, P. Sebbah, C. Vanneste, and F.

Mortessagne, *Phys. Rev. Lett.* **99**, 253902 (2007).

⁵ K. J. Vahala, *Nature* (London) **424**, 839 (2003).

⁶ G. Ramon, U. Mizrahi, N. Akopian, S. Braitbart, D. Gershoni, T. L. Reinecke, B. Gerardot, and P. M. Petroff, *Phys. Rev. B* **73**, 205330 (2006).

⁷ D. Sanvitto, A. Daraei, A. Tahraoui, M. Hopkinson, P. W. Fry, D. M. Whittaker, and M. S. Skolnick, *Appl. Phys. Lett.* **86**, 191109 (2005).

- ⁸ J. M. Gérard, B. Sermage, B. Gayral, B. Legrand, E. Costard, and V. Thierry-Mieg, *Phys. Rev. Lett.* **81**, 1110 (1998).
- ⁹ N. Akopian, N. H. Lindner, E. Poem, Y. Berlatzky, J. Avron, D. Gershoni, B. D. Gerardot, and P. M. Petroff, *Phys. Rev. Lett.* **96**, 130501 (2006).
- ¹⁰ A. Loeffler, J.P. Reithmaier, A. Forchel, A. Sauerwald, D. Peskesb, T. Kuemmel, G. Bacher, *J. Cryst. Growth* **286**, 6 (2006).
- ¹¹ H. De Raedt, A. Lagendijk, and P. de Vries, *Phys. Rev. Lett.* **62**, 47 (1989).
- ¹² T. Schwartz, G. Bartal, S. Fishman, and M. Segev, *Nature* **446**, 52 (2007).
- ¹³ J. P. Reithmaier, G. Sek, A. Löffler, C. Hofmann, S. Kuhn, S. Reitzenstein, L. V. Keldysh, V. D. Kulakovskii, T. L. Reinecke, and A. Forchel, *Nature (London)* **432**, 197 (2004).
- ¹⁴ E. Dekel, D. Gershoni, E. Ehrenfreund, D. Spektor, J. M. Garcia, and P. M. Petroff, *Phys. Rev. Lett.* **80**, 4991 (1998).
- ¹⁵ B. I. Halperin and M. Lax, *Phys. Rev.* **148**, 722 (1966).
- ¹⁶ J. Zittartz and J. S. Langer, *Phys. Rev.* **148**, 741 (1966).
- ¹⁷ E. Brezin and G. Parisi, *J. Phys. C* **13**, L307 (1980).
- ¹⁸ D. J. Thouless and M. E. Elzain, *J. Phys. C* **11**, 3425 (1978).
- ¹⁹ M. Born and E. Wolf, *Principles of Optics*, 7th ed. (Cambridge University Press, Cambridge, UK, 2003).
- ²⁰ M. E. Raikh and Al. L. Efros, *Fiz. Tverd. Tela (Leningrad)* **26**, 106 (1984) [*Sov. Phys. Solid State* **26**, 61 (1984)]; Al. L. Efros, C. Wetzel, and J. M. Worlock, *Phys. Rev. B* **52**, 8384 (1995).
- ²¹ I. M. Lifshitz, *Sov. Phys. Usp.* **7**, 549 (1965).
- ²² I. M. Lifshitz, *Adv. Phys.* **13**, 483 (1964).